Appl. Math. Mech. -Engl. Ed., **40**(9), 1313–1326 (2019)

Applied Mathematics and Mechanics (English Edition)

https://doi.org/10.1007/s10483-019-2536-9

A nonlinear model for aerodynamic configuration of wake behind horizontal-axis wind turbine*

Deshun LI[1,2,3], Tao GUO[1,2,3], Rennian LI[1,2,3,†], Congxin YANG[1,2,3], Zhaoxue CHENG[1,2,3,†], Ye LI[4,5,6,7,†], Wenrui HU[8]

1. College of Energy and Power Engineering, Lanzhou University of Technology, Lanzhou 730050, China;
2. Gansu Provincial Technology Centre for Wind Turbines, Lanzhou 730050, China;
3. Gansu Provincial Key Laboratory of Fluid Machinery and Systems, Lanzhou 730050, China;
4. School of Naval Architecture, Ocean and Civil Engineering, Shanghai Jiao Tong University, Shanghai 200240, China;
5. State Key Laboratory of Ocean Engineering, School of Naval Architecture, Ocean and Civil Engineering, Shanghai Jiao Tong University, Shanghai 200240, China;
6. Collaborative Innovation Center for Advanced Ship and Deep-Sea Exploration, Shanghai Jiao Tong University, Shanghai 200240, China;
7. Key Laboratory of Hydrodynamics (Ministry of Education), Shanghai Jiao Tong University, Shanghai 200240, China;
8. Institute of Mechanics, Chinese Academy of Sciences, Beijing 100080, China

(Received Jan. 31, 2019 / Revised Jun. 8, 2019)

Abstract Determination of the aerodynamic configuration of wake is the key to analysis and evaluation of the rotor aerodynamic characteristics of a horizontal-axis wind turbine. According to the aerodynamic configuration, the real magnitude and direction of the on-flow velocity at the rotor blade can be determined, and subsequently, the aerodynamic force on the rotor can be determined. The commonly employed wake aerodynamic models are of the cylindrical form instead of the actual expanding one. This is because the influence of the radial component of the induced velocity on the wake configuration is neglected. Therefore, this model should be called a "linear model". Using this model means that the induced velocities at the rotor blades and aerodynamic loads on them would be inexact. An approximately accurate approach is proposed in this paper to determine the so-called "nonlinear" wake aerodynamic configuration by means of the potential theory, where the influence of all three coordinate components of the induced velocity on wake aerodynamic configuration is taken into account to obtain a kind of expanding wake that

* Citation: LI, D. S., GUO, T., LI, R. N., YANG, C. X., CHENG, Z. X., LI, Y., and HU, W. R. A nonlinear model for aerodynamic configuration of wake behind horizontal-axis wind turbine. *Applied Mathematics and Mechanics* (*English Edition*), **40**(9), 1313–1326 (2019) https://doi.org/10.1007/s10483-019-2536-9

† Corresponding authors, E-mail: lirn@lut.cn, ye.li@sjtu.edu.cn, 1040809802@qq.com

Project supported by the National Basic Research Program of China (No. 2014CB046201) and the National Natural Science Foundation of China (Nos. 51766009, 51566011, and 51479114)

approximately looks like an actual one. First, the rotor aerodynamic model composed of axial (central), bound, and trailing vortexes is established with the help of the finite aspect wing theory. Then, the Biot-Savart formula for the potential flow theory is used to derive a set of integral equations to evaluate the three components of the induced velocity at any point within the wake. The numerical solution to the integral equations is found, and the loci of all elementary trailing vortex filaments behind the rotor are determined thereafter. Finally, to formulate an actual wind turbine rotor, using the nonlinear wake model, the induced velocity everywhere in the wake, especially that at the rotor blade, is obtained in the case of various tip speed ratios and compared with the wake boundary in a neutral atmospheric boundary layer. Hereby, some useful and referential conclusions are offered for the aerodynamic computation and design of the rotor of the horizontal-axis wind turbine.

Key words nonlinear wake aerodynamic model, vortex-induced velocity, integral equation of vortex-induced velocity, horizontal-axis wind turbine

Chinese Library Classification O355
2010 Mathematics Subject Classification 76B47, 35Q35, 31B10

1 Introduction

Determining an aerodynamic model for the wake behind the rotor of a horizontal-axis wind turbine is an important step towards analysis and evaluation of its aerodynamic characteristics. Actual observations, experiments, and theoretical analysis have been used to verify that the wake behind the rotor is a complicated vortex system. Different aerodynamic models of the vortex system have particular influence on the aerodynamic loads on the rotor blades. Different models result in different induced velocities at the blades so that the magnitudes, directions, and attack angles of the actual on-flows will be altered differently. Successful and simple wake aerodynamic models currently available are for a vortex system composed of helical vortex filaments on a cylindrical stream surface, for example, Glauert's model[1], Spera's model[2–3], the linear model modified from air screw[4–7], and the model presented by Madsen and Rasmussen[8]. Besides, a wake model with lifting surface description of the propeller blades has been proposed by Kerwin and Lee[9] for the design and analysis of propellers. Baltazar et al.[10] presented a numerical wake alignment method implemented in combination with the panel method. A unified lifting line method for the design and analysis of axial flow propellers and turbines was presented by Epps and Kimball[11]. Menéndez et al.[12] proposed a propeller design optimization procedure using the lifting line method to realize wake alignment. José and Falcão[13] studied the classical lifting line optimization of a horizontal-axis turbine. Melo's method[14] analyzes the flow around horizontal-axis wind turbines based on the lifting line theory and neglects the effect of the radial velocity component. Simplified models cause bigger differences with respect to the actual aerodynamic configuration of the wake and insufficient accuracy of rotor aerodynamic evaluation.

Considering these facts, a model of wake aerodynamic configuration similar to that of an actual wake is proposed in this work. Using this model, the loci of all elementary trailing vortex filaments shed from the trailing edge of the blade and the wake boundary formed by the outermost vortex filament are presented, and the induced velocity at any point within the wake is determined thereafter. Thus, a complete aerodynamic configuration of the wake is given in Fig. 1. By doing so, more accurate induced velocities at the rotor and the aerodynamic load on it can be obtained.

The solution presented herein for wake aerodynamic configuration is based on the potential theory. The air steam is assumed to be inviscid and incompressible so that the Biot-Savart law[15] can be used to calculate the velocity field induced by a spatial vortex system at any point in the flow field.

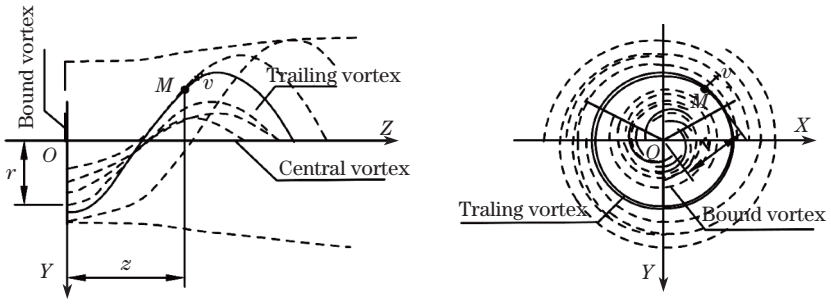

Fig. 1 Helical aerodynamic model of nonlinear wake

2 Aerodynamic model of wake

To analyze the wake configuration, a cylindrical coordinate system is established on the turbine rotor, as shown in Fig. 1. The rotor blade can be considered as a rotary wing with finite aspect[16], and the elementary vortexes shed from the blade trailing edge form a set of helical vortex sheets, whose number is equal to the number of blades. The trailing vortex sheets will propagate to an infinite distance downstream together with the air-flow (wind) while expanding outwards to form an expanding and rotating wake behind the rotor. Moreover, the blade itself will form a simplified bound vortex line (lifting line) with variable circulation. Because the vortex cannot break down in ideal fluid flow, another vortex (axial or central vortex) exists at the blade root and propagates to infinity along the rotor axis and close the vortex system. Figure 1 is a schematic diagram of the aerodynamic model of the wake composed of the aforementioned three kinds of vortexes (only one trailing vortex sheet behind a blade is depicted here).

It is logical to envisage that if only the span-wise distribution of bound vortex circulation and the loci of every elementary vortex of the trailing vortex sheet (the parametric equations are $r = r(\varphi)$ and $z = z(\varphi)$) are known, the induced velocity of the vortex system at any point within the wake (including the trailing vortex sheet) can be found with the Biot-Savart formula[15] and the potential theory. In the following paragraphs, the velocity induced by these vortexes will be analyzed in detail.

3 Induced velocity of wake vortex system

To find the induced velocity V_{id} at Point $M(r, \varphi, z)$ on an arbitrary elementary trailing vortex filament shed from the blade using the Biot-Savart formula, an auxiliary Cartesian coordinate system $Oxyz$ and a cylindrical coordinate reference system $Or\varphi Z$ are defined, as shown in Fig. 2, in which the rotor axis is the z-axis, and the blade axis is the y-axis, making the coordinate system a right-hand one.

Point M is located on the elementary vortex filament with circulation $\mathrm{d}\Gamma$ shed from the point on the blade with radius r. Its axial and radial positions are Z_M and r_M, respectively. These two parameters are the most important ones in the wake aerodynamic configuration, which can be determined only if the velocity induced by the vortex system at this point is known. The induced velocity V_{id} at this point is thus given as

$$V_{\mathrm{id}} = V_{\mathrm{c}} + V_{\mathrm{b}} + V_{\mathrm{t1}} + V_{\mathrm{t2}}, \tag{1}$$

where V_{c} denotes the velocity induced by the central (axial) vortex bundle, V_{b} is the velocity induced by the bound vortexes, V_{t1} is the velocity induced by all the elementary trailing vortex filaments shed from all the blades before Point M, and V_{t2} is the velocity induced by all the elementary trailing vortex filaments behind Point M. The trailing vortex is separated into two

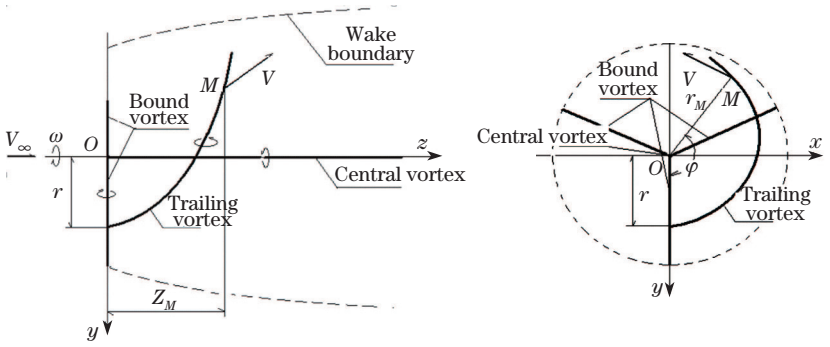

Fig. 2 Wake vortex coordinate systems

parts. All these induced velocities can be found using the Biot-Savart formula. Because V_{t1} and V_{t2} are induced by spatial helical vortex filaments, it is necessary to use the following fundamental Biot-Savart formula[8]:

$$V = \int \mathrm{d}V = \int \frac{\mathrm{d}\Gamma}{4\pi\rho^3} \int (\mathrm{d}s \times \rho). \tag{2}$$

The velocities V_c and V_b, however, can be found with the equivalent linear expression[8],

$$V = \int \mathrm{d}V = \int \frac{\mathrm{d}\Gamma}{4\pi h}(\cos\alpha + \cos\beta). \tag{3}$$

The central vortex in the wake vortex system is a linear vortex extending from the origin O to infinity behind the rotor. Using the induced velocity formula for straight vortices by the Biot-Savart law and referring to Fig. 3, the axial and radial components of the induced velocity of the central vortex at M are 0 for all three components of the cylindrical coordinate system, whereas the tangential component can only be obtained by the induced velocity formula,

$$v_c = (V_c)_z = 0, \quad w_c = (V_c)_r = 0, \quad u_c = (V_c)_\varphi = \frac{N_b \int_{r_0}^{R} \mathrm{d}\Gamma(r')}{4\pi h}(\cos\alpha + \cos\beta), \tag{4}$$

where N_b is the number of blades, and the definite integral represents the vortex strength of the bound vortex assigned to the central vortex of a blade, which is equal to the sum of the shedding vortex strengths at the trailing edge of the blade. r' is the radius of the position of the vortex beam shedding point, and h is the normal distance from Point M to the center vortex. α and β are the angles between the line from Point M to the two terminals of the central vortex and the z-axis, respectively.

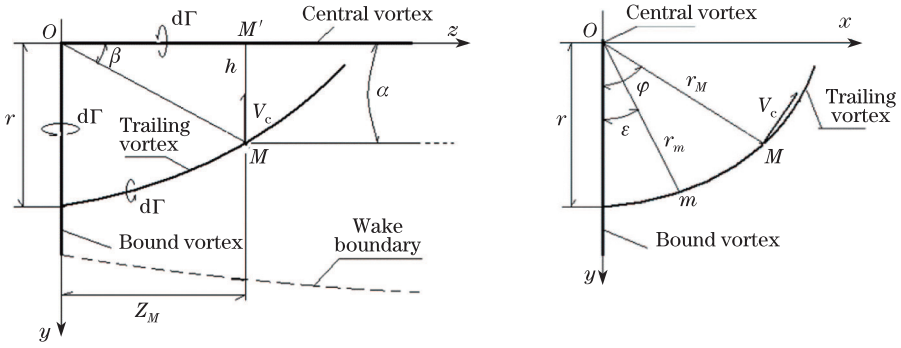

Fig. 3 Induced velocities of central vortex

The induced velocity at M is also affected by the bound vortex, as shown in Fig. 4. The bound vortex is a vortex line with changeable circulation, and the induced velocity of this vortex at M is obtained by (3). In Fig. 4, h_n is the vertical distance from M to the nth bound vortex, MQ and MQ' are, respectively, the lines from M to the two endpoints of the microsegmentation of the bound vortex, and α_n and β_n are the angles between the bound vortex line OQ_n to MQ and MQ', respectively. The parameters with subscript n are related to the nth blade.

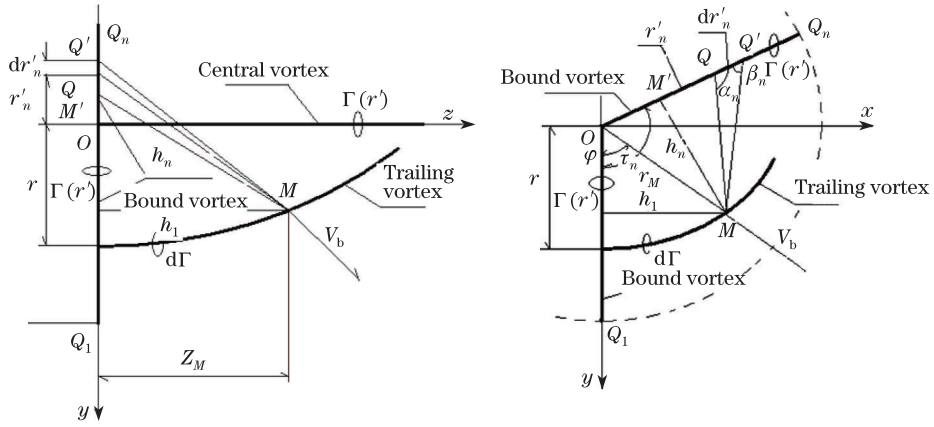

Fig. 4 Induced velocities of bound vortex

The three components of the induced velocity can be given as follows:

$$v_{\mathrm{b}} = -\frac{1}{4\pi}\int_{r_0}^{R}\Gamma(r'_n) \cdot \sum_{n=1}^{N_{\mathrm{b}}} \frac{r_M \sin(\tau_n-\varphi)}{(Z_M^2 + r_M^2\sin^2(\tau_n-\varphi))\sqrt{Z_M^2 + r'^2 + r_M^2 - 2r'r_M^2\cos(\tau_n-\varphi)}}\mathrm{d}r'_n, \tag{5}$$

$$u_{\mathrm{b}} = -\frac{1}{4\pi}\int_{r_0}^{R}\Gamma(r'_n) \cdot \sum_{n=1}^{N_{\mathrm{b}}} \frac{Z_M \cos(\tau_n-\varphi)}{(Z_M^2 + r_M^2\sin^2(\tau_n-\varphi))\sqrt{Z_M^2 + r'^2 + r_M^2 - 2r'^2r_M\cos(\tau_n-\varphi)}}\mathrm{d}r'_n, \tag{6}$$

$$w_{\mathrm{b}} = \frac{1}{4\pi}\int_{r_0}^{R}\Gamma(r'_n) \cdot \sum_{n=1}^{N_{\mathrm{b}}} \frac{Z_M \sin(\tau_n-\varphi)}{(Z_M^2 + r_M^2\sin^2(\tau_n-\varphi))\sqrt{Z_M^2 + r'^2 + r_M^2 - 2r'r_M\cos(\tau_n-\varphi)}}\mathrm{d}r'_n. \tag{7}$$

The vortex of the induced velocity at M is caused by a subsystem of trailing vortices. The bostrychoid vortex planes of N_{b} are detached from the trailing edge of each blade, which forms the subsystem of trailing vortices. The subsystem is composed of micro-vortex bunches, and each vortex bunch is located in a rotary-streamline surface of diffusion (or contraction) corresponding to the formation of a spatial vortex family. The general form of the Biot-Savart formula is used to determine the induced velocity of these infinitesimal vortex bunches at M,

$$\mathrm{d}V = \frac{\mathrm{d}\Gamma}{4\pi\rho^3}(\mathrm{d}s \times \rho). \tag{8}$$

The above formula is used on a shedding micro-vortex bunch from the trailing edge of the nth blade (see Fig. 5). (8) can be rewritten as follows:

$$(\mathrm{d}V)_n = \frac{\mathrm{d}\Gamma(r'_n)}{4\pi\rho_n^3}(\mathrm{d}s_n \times \rho_n). \tag{9}$$

$\mathrm{d}s_n$ is a micro-vortex vector of the circulation $\mathrm{d}\Gamma(r'_n)$ of a random point S_n in a vortex bunch. ρ_n is the radius vector from S_n to M, ρ_n is the mode of this radius vector, and $(\mathrm{d}V)_n$ is the induced velocity of the micro vortex at M. It should be noted that the index n refers to a corresponding physical quantity on a micro-vortex bunch that is detached from the nth blade.

The auxiliary rectangular coordinate system $Oxyz$ is used to conduct a cross product analysis of the vector, as shown in Fig. 5. In addition, to increase the calculation accuracy of the induced vortex speed, the wake vortex is divided into two parts: the front tailing vortex and the post trailing vortex.

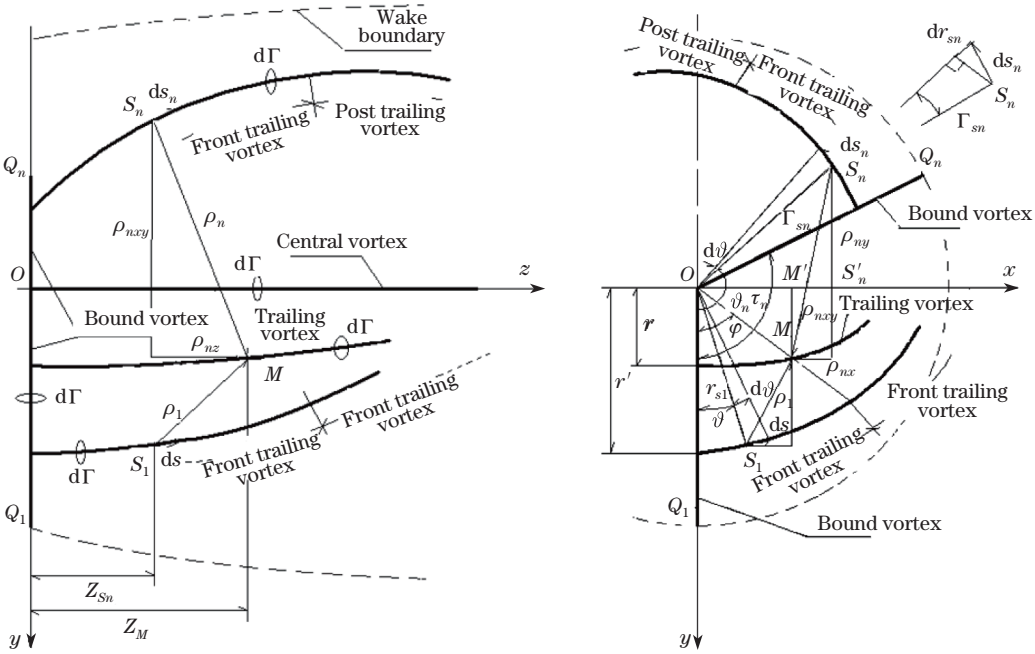

Fig. 5 Induced velocities of front trailing vortex

$V_{\mathrm{t}1}$ is the induced velocity at M of the front trailing vortex. The front trailing vortex is detached from the trailing edge of blade, and the polar angles of each point(s) on the vortex are smaller than the corresponding polar angles at M, as shown in Fig. 5. S_n is located at the deciduous vortex bunch from the trailing edge where the radial position of nth blade is $r'_n = r'$. The induced velocity $\mathrm{d}V_{\mathrm{t}1n}$ at M of the micro-vortex bunch r_0 and that of its three rectangular coordinate components $(\mathrm{d}V_{\mathrm{t}1n})_z$, $(\mathrm{d}V_{\mathrm{t}1n})_x$, and $(\mathrm{d}V_{\mathrm{t}1n})_y$ are analyzed. According to the general form of the Biot-Savart formula, given by (8), and referring to Fig. 5, the induced velocity of the front tailing vortex at M can be obtained as follows:

$$\begin{aligned} v_{\mathrm{t}1} = V_{\mathrm{t}1,z} &= \frac{1}{4\pi}\int_{r_0}^{R}\mathrm{d}\Gamma(r'_n)\int_0^{\varphi}(\mathrm{d}V_{\mathrm{t}1n})_z \\ &= \frac{1}{4\pi}\int_{r_0}^{R}\mathrm{d}\Gamma(r'_n)\sum_{n=1}^{N_{\mathrm{b}}}\int_0^{\varphi}\frac{r_{sn}r_M\cos(\varphi-\vartheta_n)-W_O r_M\sin(\varphi-\vartheta_n)-r_{sn}^2}{(r_{sn}^2-2r_{sn}r_M\cos(\varphi-\vartheta_n)+r_M^2+Z_{MSn}^2)^{\frac{3}{2}}}\mathrm{d}\vartheta, \end{aligned} \tag{10}$$

$$
\begin{aligned}
u_{\mathrm{t}1} &= V_{\mathrm{t}1,x}\cos\varphi - V_{\mathrm{t}1,y}\sin\varphi \\
&= \frac{1}{4\pi}\int_{r_0}^{R}\mathrm{d}\Gamma(r'_n) \\
&\quad\cdot\sum_{n=1}^{N_\mathrm{b}}\int_0^{\varphi}\Big(\frac{(W_O Z_{MSn}+V_O r_{sn})\cos\varphi\cos\vartheta_n - r_{sn}Z_{MSn}\cos\varphi\sin\vartheta_n - V_O r_M\cos^2\varphi}{(r_{sn}^2-2r_{sn}r_M\cos(\varphi-\vartheta_n)+r_M^2+Z_{MSn}^2)^{\frac{3}{2}}} \\
&\quad-\frac{-(W_O Z_{MSn}+V_O r_{sn})\sin\varphi\sin\vartheta_n - r_{sn}Z_{MSn}\sin\varphi\cos\vartheta_n + V_O r_M\sin^2\varphi}{(r_{sn}^2-2r_{sn}r_M\cos(\varphi-\vartheta_n)+r_M^2+Z_{MSn}^2)^{\frac{3}{2}}}\Big)\mathrm{d}\vartheta \\
&= \frac{1}{4\pi}\int_{r_0}^{R}\mathrm{d}\Gamma(r'_n) \\
&\quad\cdot\sum_{n=1}^{N_\mathrm{b}}\int_0^{\varphi}\frac{(W_O Z_{MSn}+V_O r_{sn})\cos(\varphi-\vartheta_n)+r_{sn}Z_{MSn}\sin(\varphi-\vartheta_n)-V_O r_M}{(r_{sn}^2-2r_{sn}r_M\cos(\varphi-\vartheta_n)+r_M^2+Z_{MSn}^2)^{\frac{3}{2}}}\mathrm{d}\vartheta, \qquad (11)
\end{aligned}
$$

$$
\begin{aligned}
w_{\mathrm{t}1} &= V_{\mathrm{t}1,x}\sin\varphi + V_{\mathrm{t}1,y}\cos\varphi = \frac{1}{4\pi}\int_{r_0}^{R}\mathrm{d}\Gamma(r'_n) \\
&\quad\cdot\sum_{n=1}^{N_\mathrm{b}}\int_0^{\varphi}\Big(\frac{(W_O Z_{MSn}+V_O r_{sn})\sin\varphi\cos\vartheta_n - r_{sn}Z_{MSn}\sin\varphi\sin\vartheta_n - V_O r_M\sin\varphi\cos\varphi}{(r_{sn}^2-2r_{sn}r_M\cos(\varphi-\vartheta_n)+r_M^2+Z_{MSn}^2)^{\frac{3}{2}}} \\
&\quad+\frac{-(W_O Z_{MSn}+V_O r_{sn})\cos\varphi\sin\vartheta_n - r_{sn}Z_{MSn}\cos\varphi\cos\vartheta_n + V_O r_M\cos\varphi\sin\varphi}{(r_{sn}^2-2r_{sn}r_M\cos(\varphi-\vartheta_n)+r_M^2+Z_{MSn}^2)^{\frac{3}{2}}}\Big)\mathrm{d}\vartheta \\
&= \frac{1}{4\pi}\int_{r_0}^{R}\mathrm{d}\Gamma(r'_n) \\
&\quad\cdot\sum_{n=1}^{N_\mathrm{b}}\int_0^{\varphi}\frac{(W_O Z_{MSn}+V_O r_{sn})\sin(\varphi-\vartheta_n)-r_{sn}Z_{MSn}\cos(\varphi-\vartheta_n)}{(r_{sn}^2-2r_{sn}r_M\cos(\varphi-\vartheta_n)+r_M^2+Z_{MSn}^2)^{\frac{3}{2}}}\mathrm{d}\vartheta. \qquad (12)
\end{aligned}
$$

The polar angle ϑ of S at the post trailing vortex is greater than the polar angle of M. Starting from the boundary point of the front and post trailing vortices, the polar angle ϑ will increase from 0 to the setting number of the trailing vortex ring when calculating the induced velocity at M. Therefore, the coordinate system $Oxyz$ is rotated clockwise around the z-axis, and M is located below the origin O. Oy' and Ox' are used as the new ordinate and abscissa through O and M to form a new coordinate system, as shown in Fig. 6. S_n is located at the

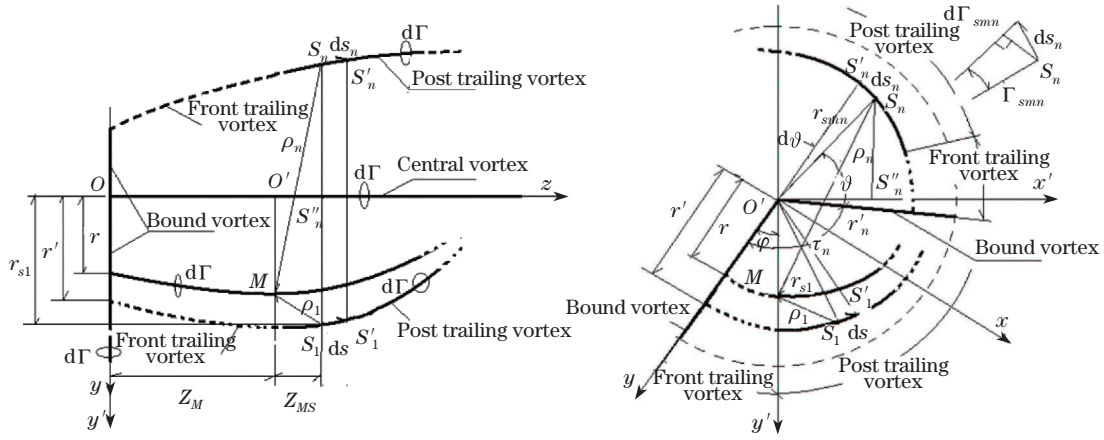

Fig. 6 Induced velocities of post trailing vortex

trailing vortex bunch of the deciduous trailing edge where the radial position of the nth blade is $r'_n = r'$. First, the induced velocity $\mathrm{d}V_{\mathrm{t}2n}$ at M of the micro-vortex bunch at S_n and that at the three rectangular coordinate components $(\mathrm{d}V_{\mathrm{t}2n})_z$, $(\mathrm{d}V_{\mathrm{t}2n})_{x'}$, and $(\mathrm{d}V_{\mathrm{t}2n})_{y'}$ are analyzed. Any physical quantity with the subscript 2 is related to the post tailing vortex and that with the subscript n is related to the nth blade. Similar to the analysis method of the front tailing vortex, the solution is based on the general form of the Biot-Savart formula given by (8),

$$v_{\mathrm{t}2} = (V_{\mathrm{t}2})_z = \frac{1}{4\pi}\int_{r_0}^{R}\mathrm{d}\Gamma(r'_n)\sum_{n=1}^{N_{\mathrm{b}}}\int_0^{\infty}\frac{r_{sn}r_M\cos\vartheta_n + W_O r_M\sin\vartheta_n - r_{sn}^2}{(r_{sn}^2 - 2r_{sn}r_M\cos\vartheta_n + r_M^2 + Z_{MSn}^2)^{\frac{3}{2}}}\mathrm{d}\vartheta, \tag{13}$$

$$u_{\mathrm{t}2} = (V_{\mathrm{t}2})_{x'} = \frac{1}{4\pi}\int_{r_0}^{R}\mathrm{d}\Gamma(r'_n) \cdot\sum_{n=1}^{N_{\mathrm{b}}}\int_0^{\infty}\frac{(V_O r_{sn} - W_O Z_{MSn})\cos\vartheta_n + r_{sn}Z_{MSn}\sin\vartheta_n - V_O r_M}{(r_{sn}^2 - 2r_{sn}r_M\cos\vartheta_n + r_M^2 + Z_{MSn}^2)^{\frac{3}{2}}}\mathrm{d}\vartheta, \tag{14}$$

$$w_{\mathrm{t}2} = (V_{\mathrm{t}2})_{y'} = \frac{1}{4\pi}\int_{r_0}^{R}\mathrm{d}\Gamma(r'_n)\sum_{n=1}^{N_{\mathrm{b}}}\int_0^{\infty}\frac{r_{sn}Z_{MSn}\cos\vartheta_n - (V_O r_{sn} - W_O Z_{MSn})\sin\vartheta_n}{(r_{sn}^2 - 2r_{sn}r_M\cos\vartheta_n + r_M^2 + Z_{MSn}^2)^{\frac{3}{2}}}\mathrm{d}\vartheta. \tag{15}$$

In the cylindrical coordinate system, the three components of the induced velocity of the center (axis) vortex, bound vortex, and trailing vortex at M and their related equations can be given. The above coordinate components of the induced velocity are summarized, and the three components of axial, tangential, and radial induced velocity of the wake vortex system at M are obtained. r' is replaced by r'_n in the above-mentioned expression, because r'_n is the same for any blade ($n = 1, 2, \cdots, N_{\mathrm{b}}$). Thus, the three components of the induced velocity can be obtained as follows:

$$\begin{aligned} v(r,\varphi) &= v_{\mathrm{c}} + v_{\mathrm{b}} + v_{\mathrm{t}1} + v_{\mathrm{t}2} \\ &= \frac{1}{4\pi}\int_{r_0}^{R}\Big(-\Gamma(r'_n)\sum_{n=1}^{N_{\mathrm{b}}}\frac{r_M\sin(\tau_n-\varphi)}{(Z_M^2 + r_M^2\sin^2(\tau_n-\varphi))\sqrt{Z_M^2 + r'^2 + r_M^2 - 2r'r_M\cos(\tau_n-\varphi)}} \\ &\quad + \frac{\mathrm{d}\Gamma(r')}{\mathrm{d}r'}\sum_{n=1}^{N_{\mathrm{b}}}\Big(\int_0^{\varphi}\frac{r_{sn}r_M\cos(\varphi-\vartheta_n) - W_O r_M\sin(\varphi-\vartheta_n) - r_{sn}^2}{(r_{sn}^2 - 2r_{sn}r_M\cos(\varphi-\vartheta_n) + r_M^2 + Z_{MSn}^2)^{\frac{3}{2}}}\mathrm{d}\vartheta \\ &\quad + \int_0^{\infty}\frac{r_{sn}r_M\cos\vartheta_n + W_O r_M\sin\vartheta_n - r_{sn}^2}{(r_{sn}^2 - 2r_{sn}r_M\cos\vartheta_n + r_M^2 + Z_{MSn}^2)^{\frac{3}{2}}}\mathrm{d}\vartheta\Big)\Big)\mathrm{d}r', \end{aligned} \tag{16}$$

$$\begin{aligned} u(r,\varphi) &= u_{\mathrm{b}} + u_{\mathrm{c}} + u_{\mathrm{t}1} + u_{\mathrm{t}2} \\ &= \frac{1}{4\pi}\int_{r_0}^{R}\Big(-\Gamma(r')\sum_{n=1}^{N_{\mathrm{b}}}\frac{Z_M\cos(\tau_n-\varphi)}{(Z_M^2 + r_M^2\sin^2(\tau_n-\varphi))\sqrt{Z_M^2 + r'^2 + r_M^2 - 2r'r_M\cos(\tau_n-\varphi)}} \\ &\quad + \frac{\mathrm{d}\Gamma(r')}{\mathrm{d}r'}\Big(\frac{N_{\mathrm{b}}}{r_M}\Big(1 + \frac{Z_M}{\sqrt{Z_M^2 + r_M^2}}\Big) \\ &\quad + \sum_{n=1}^{N_{\mathrm{b}}}\Big(\int_0^{\varphi}\frac{(W_O Z_{MSn} + V_O r_{sn})\cos(\varphi-\vartheta_n) + r_{sn}Z_{MSn}\sin(\varphi-\vartheta_n) - V_O r_M}{(r_{sn}^2 - 2r_{sn}r_M\cos(\varphi-\vartheta_n) + r_M^2 + Z_{MSn}^2)^{\frac{3}{2}}}\mathrm{d}\vartheta \\ &\quad + \int_0^{\infty}\frac{(V_O r_{sn} - W_O Z_{MSn})\cos\vartheta_n + r_{sn}Z_{MSn}\sin\vartheta_n - V_O r_M}{(r_{sn}^2 - 2r_{sn}r_M\cos\vartheta_n + r_M^2 + Z_{MSn}^2)^{\frac{3}{2}}}\mathrm{d}\vartheta\Big)\Big)\mathrm{d}r', \end{aligned} \tag{17}$$

$$
\begin{aligned}
w(r,\varphi) &= w_{\mathrm{b}} + w_{\mathrm{c}} + w_{\mathrm{t1}} + w_{\mathrm{t2}} \\
&= \frac{1}{4\pi}\int_{r_0}^{R}\Big(\Gamma(r')\sum_{n=1}^{N_{\mathrm{b}}}\frac{Z_M\sin(\tau_n-\varphi)}{(Z_M^2+r_M^2\sin^2(\tau_n-\varphi))\sqrt{Z_M^2+r'^2+r_M^2-2r'r_M\cos(\tau_n-\varphi)}} \\
&\quad + \frac{\mathrm{d}\Gamma(r')}{\mathrm{d}r'}\sum_{n=1}^{N_{\mathrm{b}}}\Big(\int_0^{\varphi}\frac{(W_O Z_{MSn}+V_O r_{sn})\sin(\varphi-\vartheta_n)-r_{sn}Z_{MSn}\cos(\varphi-\vartheta_n)}{(r_{sn}^2-2r_{sn}r_M\cos(\varphi-\vartheta_n)+r_M^2+Z_{MSn}^2)^{\frac{3}{2}}}\mathrm{d}\vartheta \\
&\quad + \int_0^{\infty}\frac{r_{sn}Z_{MSn}\cos\vartheta_n-(V_O r_{sn}-W_O Z_{MSn})\sin\vartheta_n}{(r_{sn}^2-2r_{sn}r_M\cos\vartheta_n+r_M^2+Z_{MSn}^2)^{\frac{3}{2}}}\mathrm{d}\vartheta\Big)\Big)\mathrm{d}r'. \qquad (18)
\end{aligned}
$$

The specific analytical expressions and physical meanings of the parameters in (10)–(18) are given as follows: $v(r,\varphi)$ is the axial induced velocity of the tail vortex at $M(r,\varphi)$. $u(r,\varphi)$ is the tangential induced velocity of tail vortex at $M(r,\varphi)$. $w(r,\varphi)$ is the radial induced velocity of the tail vortex at $M(r,\varphi)$. $\Gamma(r')$ is the velocity circulation at any radius r' of the blade. N_{b} is the blade number of the rotor. τ_n is the polar angle of the nth blade. Because the blades are equally spaced along the circumference, τ_n is defined as $\tau_n = \frac{2\pi}{N_{\mathrm{b}}}(n-1)$.

R is the radius of the rotor. r_0 is the non-working radius of the rotor. Each section of the blade larger than the radius is given airfoil, forming a working section. However, sections of the blade smaller than the radius are the transition sections and the journal of the blade. r is the radius of the wake vortex shedding position. The induced velocity at any position on the wake vortex beam can be obtained. r_m is the radius of the wake vortex shedding position. The micro-tailed vortex $\mathrm{d}s_n$ at any position on the wake vortex will cause an induced velocity at that location. φ is the polar angle of the rotation of the wake vortex at M. ϑ_n is the polar angle of Point S_n. $\vartheta_n = \vartheta + \tau_n$. r_M is the radial distance from M to the center vortex. The radial displacement of the trailing vortex is induced for the radial induced velocity when the trailing vortex is shed at a radial displacement r of the blade with a rotation angle φ,

$$
r_M = r + \int_0^{\varphi}\frac{w(r_m,\varepsilon)}{\omega+u(r_m,\varepsilon)/r_m}\mathrm{d}\varepsilon = r + \int_0^{\varphi} W_O\mathrm{d}\varepsilon.
$$

r_{sn} is the radial distance of S_n to the axis vortex on the front and post trailing vortices. Similar to the analysis of r_M above, the front vortex is

$$
r_{sn} = r' + \int_0^{\vartheta}\frac{w(r_m,\varepsilon)}{\omega+u(r_m,\varepsilon)/r_m}\mathrm{d}\varepsilon = r' + \int_0^{\varphi} W_O\mathrm{d}\varepsilon,
$$

and the post trailing vortex is

$$
\begin{aligned}
r_{sn} &= r' + \int_0^{\varphi}\frac{w(r_m,\varepsilon)}{\omega+u(r_m,\varepsilon)/r_m}\mathrm{d}\varepsilon + \int_0^{\vartheta}\frac{w(r_m,\varepsilon)}{\omega+u(r_m,\varepsilon)/r_m}\mathrm{d}\varepsilon \\
&= r' + \int_0^{\varphi} W_O\mathrm{d}\varepsilon + \int_0^{\vartheta} W_O\mathrm{d}\varepsilon.
\end{aligned}
$$

W_O is the signum function representing the integrand of radial displacement,

$$
W_O = \frac{w(r_m,\varepsilon)}{\omega+u(r_m,\varepsilon)/r_m}.
$$

Z_M is the axial displacement of M. The point of the deciduous trailing vortex at the radial position r of blades moves with $V_\infty + v(r_m,\varepsilon)$ for the axial induced velocity. The total displacement to M is

$$
Z_M = \int_0^{\varphi}\frac{V_\infty + v(r_m,\varepsilon)}{\omega+u(r_m,\varepsilon)/r_m}\mathrm{d}\varepsilon = \int_0^{\varphi} V_O\mathrm{d}\varepsilon.
$$

V_O is the signum function representing the integrand of axial displacement,

$$V_O = \frac{V_\infty + v(r_m, \varepsilon)}{\omega + u(r_m, \varepsilon)/r_m}.$$

Z_{MSn} is the axial component of the radius vector S_nM, which is the difference in the axial displacement M and S_n,

$$Z_{MSn} = \begin{cases} \displaystyle\int_\vartheta^\varphi \frac{V_\infty + v(r_m, \varepsilon)}{\omega + u(r_m, \varepsilon)/r_m}\mathrm{d}\varepsilon = \int_\vartheta^\varphi V_O \mathrm{d}\varepsilon & \text{for the front trailing vortex,} \\ \displaystyle\int_0^\vartheta \frac{V_\infty + v(r_m, \varepsilon)}{\omega + u(r_m, \varepsilon)/r_m}\mathrm{d}\varepsilon = \int_0^\vartheta V_O \mathrm{d}\varepsilon & \text{for the post trailing vortex.} \end{cases}$$

All parameters in the under-mentioned expressions are dimensionless quantities[5]. The specific method is as follows: the dimensionless radial and axial lengthes are their ratios to the rotor radius R, each velocity quantity is its ratio to ωR, and circulation is its ratio to $4\pi\omega R^2$. For example, the dimensionless radius is $\overline{r} = r/R$. The dimensionless axial induced velocity is $\overline{v}(r,\varphi) = v(r,\varphi)/(\omega R)$. The dimensionless circulation is $\overline{\Gamma}(\overline{r}') = \Gamma(r')/(4\pi\omega R^2)$. Finally, all overlines are removed to obtain the general form. The expressions of the three cylindrical coordinate components of induced velocity are given as follows:

$$\begin{aligned} v(r,\varphi) = \int_{r_0}^1 \Big(& -\Gamma(r') \sum_{n=1}^{N_\mathrm{b}} \frac{r_M \sin(\tau_n - \varphi)}{(Z_M^2 + r_M^2 \sin^2(\tau_n - \varphi))\sqrt{Z_M^2 + r'^2 + r_M^2 - 2r'r_M\cos(\tau_n - \varphi)}} \\ & + \frac{\mathrm{d}\Gamma(r')}{\mathrm{d}r'} \sum_{n=1}^{N_\mathrm{b}} \Big(\int_0^\varphi \frac{(r_{sn} r_M \cos(\varphi - \vartheta_n) - W_O r_M \sin(\varphi - \vartheta_n) - r_{sn}^2)}{(r_{sn}^2 - 2r_{sn}r_M\cos(\varphi - \vartheta_n) + r_M^2 + Z_{MSn}^2)^{\frac{3}{2}}}\mathrm{d}\vartheta \\ & + \int_0^\infty \frac{(r_{sn} r_M \cos\vartheta_n + W_O r_M \sin\vartheta_n - r_{sn}^2}{(r_{sn}^2 - 2r_{sn}r_M\cos\vartheta_n + r_M^2 + Z_{MSn}^2)^{\frac{3}{2}}}\mathrm{d}\vartheta \Big)\Big)\mathrm{d}r', \end{aligned} \tag{19}$$

$$\begin{aligned} u(r,\varphi) = \int_{r_0}^1 \Big(& -\Gamma(r') \sum_{n=1}^{N_\mathrm{b}} \frac{Z_M \cos(\tau_n - \varphi)}{(Z_M^2 + r_M^2 \sin^2(\tau_n - \varphi))\sqrt{Z_M^2 + r'^2 + r_M^2 - 2r'r_M\cos(\tau_n - \varphi)}} \\ & + \frac{1}{4\pi}\frac{\mathrm{d}\Gamma(r')}{\mathrm{d}r'}\Big(\frac{N_\mathrm{b}}{r_M}\Big(1 + \frac{Z_M}{\sqrt{Z_M^2 + r_M^2}}\Big) \\ & + \sum_{n=1}^{N_\mathrm{b}} \Big(\int_0^\varphi \frac{(W_O Z_{MSn} + V_O r_{sn})\cos(\varphi - \vartheta_n) + r_{sn} Z_{MSn}\sin(\varphi - \vartheta_n) - V_O r_M}{(r_{sn}^2 - 2r_{sn}r_M\cos(\varphi - \vartheta_n) + r_M^2 + Z_{MSn}^2)^{\frac{3}{2}}}\mathrm{d}\vartheta \\ & + \int_0^\infty \frac{(V_O r_{sn} - W_O Z_{MSn})\cos\vartheta_n + r_{sn} Z_{MSn}\sin\vartheta_n - V_O r_M}{(r_{sn}^2 - 2r_{sn}r_M\cos\vartheta_n + r_M^2 + Z_{MSn}^2)^{\frac{3}{2}}}\mathrm{d}\vartheta \Big)\Big)\Big)\mathrm{d}r', \end{aligned} \tag{20}$$

$$\begin{aligned} w(r,\varphi) = \int_{r_0}^1 \Big(& \Gamma(r') \sum_{n=1}^{N_\mathrm{b}} \frac{r_M \sin(\tau_n - \varphi)\cos(\tau_n - \varphi)}{(Z_M^2 + r_M^2 \sin^2(\tau_n - \varphi))\sqrt{Z_M^2 + r'^2 + r_M^2 - 2r'r_M\cos(\tau_n - \varphi)}} \\ & + \frac{\mathrm{d}\Gamma(r')}{\mathrm{d}r'} \sum_{n=1}^{N_\mathrm{b}} \Big(\int_0^\varphi \frac{(W_O Z_{MSn} + V_O r_{sn})\sin(\varphi - \vartheta_n) - r_{sn} Z_{MSn}\cos(\varphi - \vartheta_n)}{(r_{sn}^2 - 2r_{sn}r_M\cos(\varphi - \vartheta_n) + r_M^2 + Z_{MSn}^2)^{\frac{3}{2}}}\mathrm{d}\vartheta \\ & + \int_0^\infty \frac{r_{sn} Z_{MSn}\cos\vartheta_n - (V_O r_{sn} - W_O Z_{MSn})\sin\vartheta_n}{(r_{sn}^2 - 2r_{sn}r_M\cos\vartheta_n + r_M^2 + Z_{MSn}^2)^{\frac{3}{2}}}\mathrm{d}\vartheta \Big)\Big)\mathrm{d}r'. \end{aligned} \tag{21}$$

The analytical expressions of the key parameters in the above-mentioned expressions of the induced velocity components are as follows:

$$r_M = r + \int_0^{\varphi} \frac{w(r_m,\varepsilon)}{1+u(r_m,\varepsilon)/r_m}\mathrm{d}\varepsilon, \tag{22}$$

$$r_{sn} = \begin{cases} r' + \displaystyle\int_0^{\vartheta} \frac{w(r_{sn},\varepsilon)}{1+u(r_{sn},\varepsilon)/r_{sn}}\mathrm{d}\varepsilon \quad \text{for the front trailing vortex,} \\ r' + \displaystyle\int_0^{\varphi} \frac{w(r_{sn},\varepsilon)}{1+u(r_{sn},\varepsilon)/r_{sn}}\mathrm{d}\varepsilon \\ \quad + \displaystyle\int_0^{\vartheta} \frac{w(r_{sn},\varepsilon)}{1+u(r_{sn},\varepsilon)/r_{sn}}\mathrm{d}\varepsilon \quad \text{for the post trailing vortex,} \end{cases} \tag{23}$$

$$Z_{MSn} = \begin{cases} \displaystyle\int_{\theta}^{\varphi} \frac{\frac{1}{\lambda_0}+v(r_m,\varepsilon)}{1+u(r_m,\varepsilon)/r_m}\mathrm{d}\varepsilon \quad \text{for the front trailing vortex,} \\ \displaystyle\int_0^{\infty} \frac{\frac{1}{\lambda_0}+v(r_m,\varepsilon)}{1+u(r_m,\varepsilon)/r_m}\mathrm{d}\varepsilon \quad \text{for the post trailing vortex,} \end{cases} \tag{24}$$

$$W_O = \frac{w(r_m,\varepsilon)}{1+u(r_m,\varepsilon)/r_m}, \quad V_O = \frac{\frac{1}{\lambda_0}+v(r_m,\varepsilon)}{1+u(r_m,\varepsilon)/r_m}. \tag{25}$$

It can be seen from (19)–(21) that the analytical expressions of the three components of induced velocity are, in fact, a set of nonlinear integral equations (there are unknown variables, or their integrals are on the right side of the equations). In the wind turbine wake vortex system, the dimensionless expressions (19)–(25) of the induced velocity and parameter at any wake vortex can be solved. Because integral equations are extremely complicated, it is more feasible to employ a numerical solution with an iterative approximation.

4 Illustration of nonlinear wake aerodynamic configuration and its analysis

A 33 kW rotor of a horizontal-axis wind turbine was used to illustrate the approximation calculation of its wake aerodynamic configuration under various tip speed ratios by using the proposed method. The wind turbine adopts the field test unit developed at Lanzhou University of Technology. The turbine is a horizontal-axis two-blade upwind-type turbine. It has a diameter of 14.8 m, hub height of 15.4 m, rated wind speed of 11 m/s, rated speed of 85 r/min, and National Advisory Committee for Aeronautics (NACA) series airfoils. The specific blade parameters are shown in Table 1.

Table 1 Position and geometric parameters of six airfoils

Airfoil number	Relative radial position/%	Initial setting angle/(°)	Chord length/mm	Airfoil
#1	96.53	–54.839 7	213.63	NACA4415
#2	89.84	–55.790 8	237.48	NACA4418
#3	79.84	–56.929 9	283.12	NACA4421
#4	64.84	–59.031 6	350.16	NACA4424
#5	49.77	–60.479 1	414.36	NACA4427
#6	34.23	–62.734 5	485.63	NACA4430

Under the assumption of potential flow of the wake, a vortex aerodynamic model of the rotor (cylinder tail vortex model) is first established. Then, the aerodynamic structure of the rotor wake can be obtained with the iterative approximation method using the Biot-Savart vortex-inducing velocity formula, which presents the distribution of the spiral wake vortex and velocity field. Figure 7 shows the aerodynamic structure of the wake under three different operating

conditions with tip speed ratios of $\lambda_0 = 3$, 6, and 9. With an increase in the tip speed ratio, the curvature of the wake boundary increases, and the contraction of the center vortex becomes more evident.

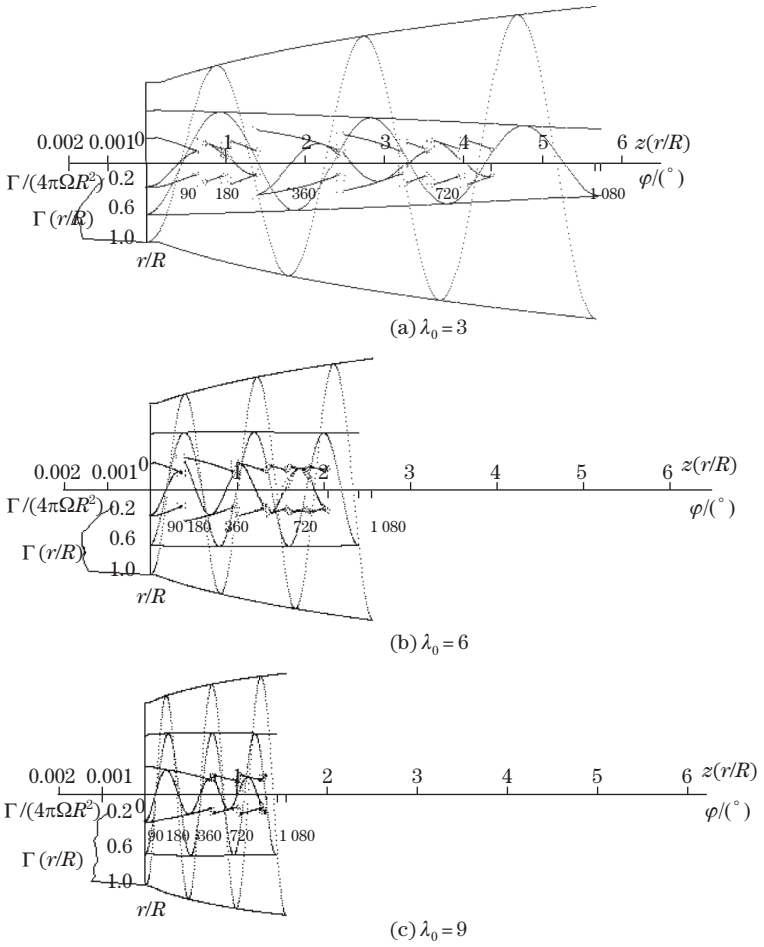

Fig. 7 Wake boundary and three wake vortex beam trajectories

The large eddy simulation (LES) method combined with the actuator line model is used, and the wake of the wind turbine with different tip speed ratios is simulated in the neutral atmospheric boundary layer to verify the accuracy of the nonlinear wake boundary. In addition, the above numerical methods are verified by the field experimental data (see Refs. [17] and [18] for details). An outline chart of the wake velocity under different tip speed ratios ($\lambda_0 = 3$, 6, and 9) in the neutral atmospheric boundary layer is shown in Fig. 8. The horizontal profile of the time-averaged velocity at the hub height is extracted at multiple locations downstream of the rotor ($1 \leqslant L/R \leqslant 6$). D and R are the diameter and radius of the rotor, respectively, and the ordinate r/D represents the relative distance from the rotor axis. The abscissa U/U_0 represents the wake dimensionless velocity, and U_0 is the average velocity of the inflow. The wake velocity returns to 99% of the incoming flow velocity, which indicates that the wake has regained to that of the atmospheric state. Thus, the black dotted lines in the figure represent the boundary of the wake velocity. With an increase in the tip speed ratio, the curvature of the boundary line increases. In addition, the non-uniformity of atmospheric inflow leads to asymmetry in the wake. The red lines represent the boundary of the nonlinear trailing vortex.

A comparison of this with the wake boundary in the neutral atmospheric boundary layer shows that the two boundaries are essentially consistent with each other. However, the expansion of wake in the neutral atmospheric boundary layer is slightly greater. Taking the nonlinear wake boundary as the standard, when the tip speed ratio is 3, 6, and 9, the deviations in the two boundaries are 3.1%–8.1%, 3.7%–6.9%, and 7.7%–9.7%, respectively. These results further prove that the nonlinear trailing vortex model can well describe the wake boundary in neutral atmospheric conditions.

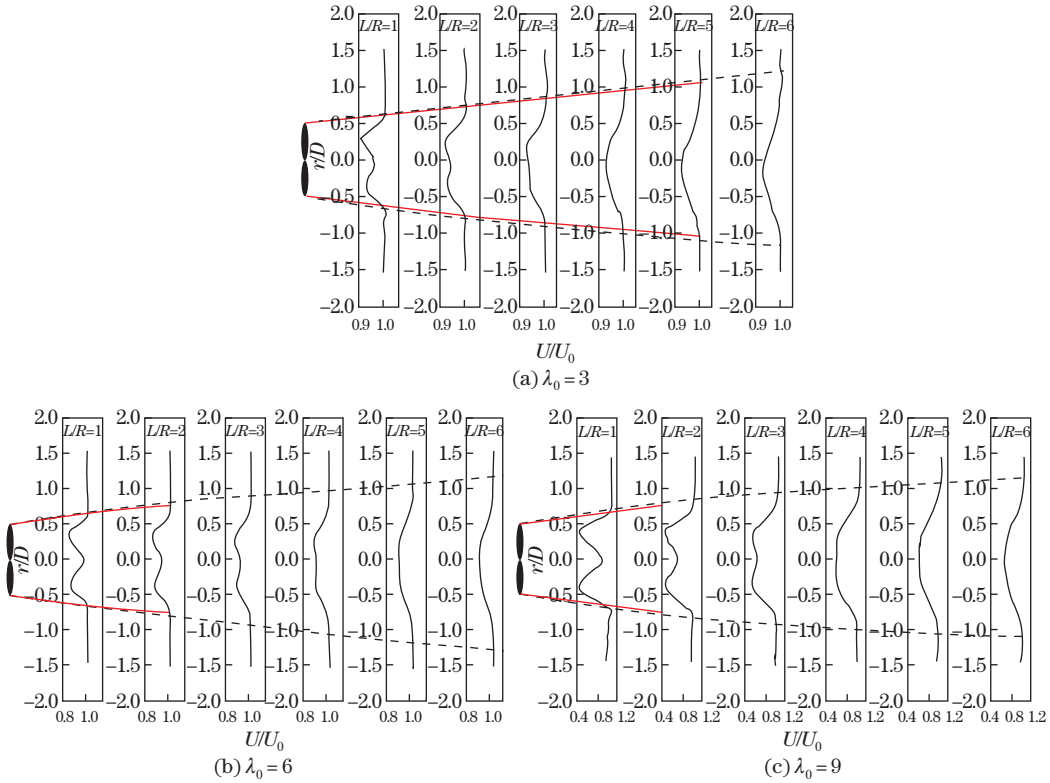

Fig. 8 Spanwise distributions of time-averaged velocity of different tip speed ratios (color online)

5 Conclusions

It is possible to determine the aerodynamic configuration of wake behind the rotor of a horizontal-axis wind turbine on the basis of potential theory, where the influence of all three coordinate components of the induced velocity on the wake aerodynamic configuration is taken into account, particularly the effect of the radial induced velocity on the wake expansion. Thus, a type of expanding wake that approximately resembles an actual wake can be obtained. Further, the change law of the wake boundary of a wind turbine in the neutral atmospheric boundary layer can be well described by it. The accuracy of the proposed method is evidently restricted by the presumption of an ideal fluid. Nevertheless, this potential flow approach does have certain practical value in the evaluation of aerodynamic characteristics of wind turbine rotors considering that almost all existing aerodynamic computation and design methods for wind turbine rotors are based on the potential theory.

References

[1] GOURIERES, D. L. Wind power plants. *Theory and Design*, Pergamon Press, Oxford (1982)

[2] SPERA, S. D. A. *Wind Turbine Technology*: *Fundamental Concepts of Wind Turbine Engineering*, ASME Press, New York (1994)

[3] EGGLESTON, D. M. and STODDART, F. S. *Wind Turbine Engineering Design*, Van Nostrand, New York (1987)

[4] BURTON, T., SHARPE, D., and JENKINS, N. *Wind Energy Handbook*, John Wiley & Sons, Chichester (2001)

[5] CHENG, Z. X., LI, R. N., YANG, C. X., and HU, W. R. Criterion of aerodynamic performance of large-scale offshore horizontal-axis wind turbines. *Applied Mathematics and Mechanics* (*English Edition*), **31**(1), 13–20 (2010) https://doi.org/10.1007/s10483-010-0102-2

[6] CHENG, Z. X., YE, Z. Q., CHEN, J. Y., and BAI, S. B. Aerodynamic optimization for the rotor of horizontal-axis wind machine. *Proceedings of International Conference on New and Renewable Energy*, 306–312 (1990)

[7] YE, Z. Q., CHENG, Z. X., CHEN, J. Y., and BAI, S. B. Aerodynamic optimum design procedure and program for the rotor of a horizontal-axis wind turbine. *Wind Engineering and Industrial Aerodynamics*, **39**, 179–186 (1992)

[8] MADSEN, H. A. and RASMUSSEN, F. A. Near wake model for trailing vorticity compared with the blade element momentum theory. *Wind Energy*, **7**, 325–341 (2004)

[9] KERWIN, J. and LEE, C. S. Prediction of a steady and unsteady marine propeller performance by numerical lifting-surface theory. *SNAME Transactions*, **86**, 218–253 (1978)

[10] BALTAZAR, J., FALCAO DE CAMPOS, J. A. C., and BOSSCHERS, J. Open-water thrust and torque predictions of a ducted propeller system with a panel method. *International Journal of Rotating Machinery*, **2012**(2), 67–74 (2012)

[11] EPPS, B. P. and KIMBALL, R. W. Unified rotor lifting line theory. *Journal of Ship Research*, **57**(4), 181–201 (2013)

[12] MENÉNDEZ, A., DAVID, H., and KINNAS, S. A. On fully aligned lifting line model for propellers: an assessment of Betz condition. *Journal of Ship Research*, **58**(3), 130–145 (2014)

[13] JOSÉ, A. C. and FALCÃO, D. C. Hydrodynamic power optimization of a horizontal axis marine current turbine with lifting line theory. *The Seventeenth International Offshore and Polar Engineering Conference*, International Society of Offshore and Polar Engineers, Lisbon (2007)

[14] MELO, D. B., BALTAZAR, J., and FALCAO DE CAMPOS, J. A. C. A numerical wake alignment method for horizontal axis wind turbines with the lifting line theory. *Journal of Wind Engineering and Industrial Aerodynamics*, **174**, 382–390 (2018)

[15] MARGERIT, D. and BRANCHER, J. P. Asymptotic expansions of the Biot-Savart law for a slender vortex with core variation. *Journal of Engineering Mathematics*, **40**(3), 279–313 (2001)

[16] JOHNSON, W. Recent developments in rotary-wing aerodynamic theory. *AIAA Journal*, **24**(8), 1219–1244 (1986)

[17] LI, D. S., GUO, T., LI, Y. R., HU, J. S., ZHENG, Z., LI, Y., DI, Y. J., HU, W. R., and LI, R. N. Interaction between the atmospheric boundary layer and a standalone wind turbine in Gansu — part I: field measurement. *Science China Physics, Mechanics and Astronomy*, **61**, 94711 (2018)

[18] ZHENG, Z., GAO, Z. T., LI, D. S., LI, R. N., LI, Y, HU, Q. H., and HU, W. R. Interaction between the atmospheric boundary layer and a stand-alone wind turbine in Gansu — part II: numerical analysis. *Science China Physics, Mechanics and Astronomy*, **61**, 94712 (2018)